A PGD-based Multiscale Formulation for Non-Linear Solid Mechanics Under Small Deformations

F. El Halabi[a], D. González[c,*], J. A. Sanz-Herrera[d], M. Doblaré[b,d]

[a] *Research Centre for Energy Resources and Consumption (CIRCE) Universidad de Zaragoza, CIRCE Building, Campus Río Ebro, Zaragoza, Spain*
[b] *Group of Structural Mechanics and Materials Modelling (GEMM) Aragon Institute of Engineering Research (I3A), University of Zaragoza, Spain*
[c] *Aragon Institute of Engineering Research (I3A), University of Zaragoza, Spain*
[d] *Abengoa Research, Sevilla , Spain*

Abstract

Model reduction techniques have became an attractive and a promising field to be applied in multiscale methods. The main objective of this work is to formulate a multiscale procedure for non-linear problems based on parametrized microscale models. The novelty of this work relies in the implementation of the model reduction technique known as Proper Generalized Decomposition for solving the high dimensional parametrized problem resulting from the microscale model. The multiscale framework here proposed is formulated to non-linear problems, specifically to material non-linearities, where material response is governed by a strain dependent evolution law. Two strategies to deal with this kind of problem under small deformations are detailed in this work. Both strategies based on parametrized microscale models solved by PGD have been applied to a problem with a rate-dependent isotropic damage model. First, a procedure where the problem is solved by uncoupling the equilibrium equation to the state variable expression has been explored. In order, to alleviate the parametrized microscale problem, a second strategy for problems with material non-linearity has been proposed, incorporating a parametrized microscale problem at each macroscale increment (FE-PGD). The basis of those procedures are described and compared, highlighting the solution accuracy and computer time consumption in comparison to a traditional finite element analysis.

*Phone: (+34) 608 226309; *e-mail*: gonzal@unizar.es

Keywords: Proper Generalized Decomposition, Multi-scale, Non-Linear Solid Mechanic, Damage, Reduced Order Model

1. Introduction

Multiscale modelling is aimed to alleviate computational costs in problems where local solution involves phenomena with a short length of variation in space and/or time, that are generally prohibitive if a brute computational force is used by meshing the whole domain, including all heterogeneities. Multiscale methodologies try to solve this kind of problems by computing material properties or system behavior on a coarse scale using information or models from finer scales. On each scale, particular approaches are used for describing the system and consequently to reduce the computational cost.

In the literature many classifications of multiscale approaches can be found. Usually, they are classified into two main families, namely hierarchical and concurrent [1, 2]. In hierarchical approaches, the behavior at the macroscale is obtained from the solution of a boundary value problem solved at the microscale, represented by a representative volume element of the material. This behavior can be determined under the form of macroscopic constitutive relations whose effective properties are identified from the solution of the microscopic problem. In this category micromechanical approaches can be found [3]. The microscopic solution can also be incorporated into the macroscopic problem through different numerical schemes. It can be condensed at the macroscale as in the case of the variational multiscale method [4], or within a decomposition domain framework for structural mechanics applications [5]. One of the major feature of hierarchical approaches is that the microscopic problems can be solved once for all, and consequently that only a finite number of microscopic solutions have to be known, that is the case of asymptotic homogenization theories [6].

By contrast, in concurrent approaches the microscopic and macroscopic scales are solved simultaneously. This is required when the macroscopic behavior can not be obtained explicitly, which occurs as soon as microscopic nonlinear behavior is involved. These methods were reviewed in [7] in the continuum mechanics framework. The most popular approach is the Multilevel Finite Element method (FE^2) initiated by Feyel in [8], which has also

be named later as computational homogenization. As noticed in [1], both the hierarchical and concurrent simulation approaches offer cost savings over large scale direct numerical simulation of the microstructure. However, efforts are directed towards improving their numerical efficiency.

For linear problems, asymptotic homogenization theories with periodic boundary conditions have become into the most used and successful approach enabling obtaining both the local state in the RVE and the global solution in the two scales [6, 9, 10]. This method however presents several drawbacks. First, a strong accuracy reduction might be expected when actual periodicity of the microstructure is lost; second, the boundary regions where the material cannot be homogenized require special attention [11, 9] and, finally, its application to non-linear material behavior is costly. As a matter of fact, extending this theory to microstructure evolving nonlinear problems implies the need of modelling the whole domain and each RVE for each load (or time) step, thus obtaining the homogenized (averaged) macroscopic material properties at each local point and time [12, 13, 14, 15]. After solving the macroscopic problem, the values of the connecting variables are transferred (restricted) to the micro-RVE that is then solved and, if needed, its microstructure and properties updated. This procedure is often denoted as computational homogenization or, when using finite element approximation, multi-level finite element method (FE^2).

The multiscale procedure here proposed is based on the technique presented in [16] where the solution is represented through an additive splitting of displacement field between the macroscale solution and a microscale one with homogeneous boundary conditions. Furthermore, no homogenization operator is needed, but, as in Variational Multiscale [4], the microstructure domain RVE is identified with an element of the macroscale discretization. As in [16], the novelty lies in the fact that the microscale problem is here solved in a previous "off-line" step in which a reference RVE is solved for any possible set of geometry, material properties and *restricted* variables. The resulting solution is used as microscale information and then "prolonged" (averaged) for any possible set of geometry or restricted variables, thus obtaining all variables needed at the macroscale without the need of explicitly solving each RVE during the microscale stage of the FE^2 approach, since it is solved in advance.

Two different multiscale strategies based on microscale models solved by the PGD technique (section 2) for small deformation non-linear problems are formulated in section 3. Finally, a problem with rate-dependent isotropic damage model solved through the proposed multiscale strategies is presented in section 4, which results have been compared with those obtained through a traditional finite element procedure.

2. The Proper Generalized Decomposition (PGD) technique

The PGD technique aims to approximate the solution by means of a sum of products (sometimes called finite sum decomposition) of separated functions depending on each of the problem dimension or parameter. The PGD method can be found in different contexts: parametrized PDEs [17, 18, 19], parametric modeling and structural optimization [20], separation of coordinate variables in multi-dimensional PDEs [21, 22, 23, 24], among some others. Recently, pioneers authors of this technique proposed several formulations applying this scheme to multiscale problems [25, 26, 27, 28]. Furthermore, a time multiscale procedure based in PGD was proposed in [27] to deal with problems where a very fine time discretization is demanded.

As mentioned before, the approximation of the variable function by means of PGD is constructed by means of a sum of products of separated one-dimensional functions depending on each of the problem dimensions or parameters. Each of these functions is determined by an iterative approach, with no initial assumption on their global form, although most of the times, they are expressed as piecewise functions with small support as in standard one-dimensional finite elements. Let $\psi(\mathbf{z})$ be a scalar function of $\mathbf{z} = (z_1, z_2, \cdots, z_D) \in \Omega = \prod_{k=1}^{D}[l_k, L_k]$. In the PGD approach, this function is approximated as:

$$\psi(\mathbf{z}) \approx \sum_{i=1}^{I} \prod_{k=1}^{D} F_i^k(z_k) \tag{1}$$

with $F_i^k(z_k)$ the $i-th$ one-dimensional function of the $k-th$ variable z_k, that has to be determined along the process, D the number of independent variables (dimensions) and I the number of summands (terms) of the approximation. As commented, each of the functions $F_i^k(z_k)$ is usually expressed in

discrete form, as in one-dimensional finite elements, by means of a piecewise linear (or any higher order) interpolation as:

$$F_i^k(z_k) = \sum_{n=1}^{M_k} N^n(z_k) F_{in}^k \tag{2}$$

with $N^n(z_k)$ the standard linear one-dimensional spline shape function with value 1 at the associated node n and zero at the rest of the M_k nodes of the chosen discretization in the interval $[l_k, L_k]$, F_{in}^k represents the nodal value of the function F_i^k at node n. From (1), solving a D-dimensional problem with M nodes discretizing each dimension ($M = M_k$ $(k = 1, \ldots, D)$, without loss of generality), the total number of unknowns involved in the solution is $M \cdot D \cdot I$, where I is the number of terms of the separated representation, instead of the M^D degrees of freedom involved in mesh based discretizations. As it can be noticed in the expression of the separated representation, the complexity scales linearly with the dimension of the space in which the model is defined, from which advantage can be taken for building more efficient parametrized models. In general, for many models, the number of terms I in the finite sum is quite reduced (few tens) [28], the number of terms of the finite sum is strongly associated to the number of separated variables (problem dimension) and to problem non-linearity.

3. Microscale Parametrized Models for Non-linear Analysis

Problems that present material non-linearity, history dependency or where the behavior parameters vary at each point with the local level of deformation, need an incremental procedure for its resolution. In this work, two different procedures to solve problems with material non-linearities based on microscale parametrized models are formulated. First, a general formulation based on uncoupling the non-linear set of equations is presented. Thus, material governing and equilibrium equations are parametrized in a general sense at an "off-line" microscale step. Then, the microscale parametrized results can be particularized at the macroscale for a specific set of independent variables. In the second strategy, an alleviation of the microscale "off-line" step is achieved by incorporating into the macroscale incremental analysis a reduced microscale parametrized problem. This has been denoted as a $FE - PGD$ procedure. In the subsequent subsections both formulations are

detailed.

3.1. 1st Strategy: Micro-step Uncoupling Equilibrium and Evolution Equations

The goal of the proposed multiscale strategy is to formulate and solve in an "off-line" step, parametrized microscale models to alleviate the computational cost of the macroscale problem. The microscale parametrized model has to be able to accurately compute the resulting displacement field for different material properties (internal variable) distributions and boundary conditions associated to a specific state. For instance, let us consider the following equilibrium problem with a material non-linearity:

$$\nabla \cdot \mathbf{D}(\boldsymbol{\kappa}(\boldsymbol{\varepsilon})) \cdot \boldsymbol{\varepsilon}(\mathbf{u}) + \mathbf{f} = 0 \tag{3}$$

$$\mathfrak{F}(\mathbf{D}(\boldsymbol{\kappa}(\boldsymbol{\varepsilon})) = \boldsymbol{\Psi}(\boldsymbol{\varepsilon}, \boldsymbol{\kappa}) \tag{4}$$

Here, $\mathbf{u}$, $\boldsymbol{\varepsilon}$ and $\boldsymbol{\kappa}$ represent the displacement vector, strain and internal variable at a point $\mathbf{x} \in \Omega$, respectively. $\mathbf{D}$ and $\mathbf{f}$ represent the stiffness matrix and body force vector (force per unit volume), respectively. Function $\boldsymbol{\Psi}$ defines the relation between the elastic property and the strain state of point $\mathbf{x}$.

Small deformation is considered in the microscale parametrized problem where the equilibrium problem and material characteristic behavior are solved uncoupled. Thus, both expressions can be parametrized separately in "off-line" steps to then be particularized at the macro problem for each RVE. Consequently, the boundary value problem for the microscale model must be parametrized for a sufficient generic distribution of the desired internal variable ($\boldsymbol{\kappa}$), that will be governed by the stain/stress state. The problem can be solved by considering the material property/internal variable in each microscale node or spatial region as an additional variable in the parametrization. Then the material property/internal variable function will be approximated in an interpolation manner over the microdomain:

$$E(\mathbf{x}) = \mathbf{N}^T \hat{\mathbf{E}} \tag{5}$$

taking each nodal value description $\hat{E}_i$ as an extra parameter.

The microscale parametrized problem is built in such a manner that the displacement field distribution over the micro model for any combination

(within a predefine range) of displacement boundary condition and material property/internal variable distribution can be computed. For instance, considering an isotropic material which matrix of elasticity $\mathbf{D}$ can be represented as:

$$\mathbf{D}(\mathbf{x}, \boldsymbol{\kappa}) = E(\mathbf{x}, \boldsymbol{\kappa})\tilde{\mathbf{D}} \tag{6}$$

where, $E(\mathbf{x}, \boldsymbol{\kappa})$ is the a spatial and internal variable dependent elastic modulus. For this case, the displacement variable will be approximated as follows

$$\mathbf{u} = \sum_{i=1}^{I} \mathbf{a}_i(\mathbf{x}) \prod_{k=1}^{D} G_i^k(z_k) \prod_{p=1}^{P} H_i^p(e_p) \tag{7}$$

where $\mathbf{a}_i(\mathbf{x})$ represents the n-dimensional i-th function of the approximation that depends on the coordinates vector $\mathbf{x}$. This basis function will be approximated again as in typical finite elements [29]. $G_i^k(z_k)$ are the i-th function of the approximation that depends on the k-th variable, D is assumed to be the number of variables associated to the Dirichlet boundary condition approximation [16]. $H_i^p(e_p)$ are the i-th function of the approximation that depends on the p-th variable, here, P represents the number of variables associated to the nodal material property. Note that if a finite element approximation of material property distribution is used, thus, P is equal to the number of nodes in the RVE discretization. The material property/internal variable is approximated as a sum of separated functions describing in each one the spatial dependency and parametrized range value of the material property distribution, then this approximation can be written as,

$$E(\mathbf{x}, e_P) = \sum_{p=1}^{P} E_p(\mathbf{x}, e_p) = \sum_{p=1}^{P} \mathbf{c}_p(\mathbf{x}) L_p(e_p) \tag{8}$$

In (8), functions $\mathbf{c}_p$ active node p in each sum that will be associated to function $L_p(e_p)$, i.e., the spatial distribution for a bidimensional problem, $E(\mathbf{x}, e_P)$ can be written in a separated format as,

$$\begin{aligned} &\sum_{p=1}^{P} \mathbf{c}_p(\mathbf{x}) L_p(e_p) = \mathbf{c}_1 \cdot L_1 + \cdots + \mathbf{c}_p \cdot L_p = \\ &\begin{pmatrix} 1 \\ 1 \\ \mathbf{0} \end{pmatrix} \cdot L_1 + \begin{pmatrix} 0 \\ 0 \\ 1 \\ 1 \\ \mathbf{0} \end{pmatrix} \cdot L_2 + \cdots + \begin{pmatrix} \mathbf{0} \\ 1 \\ 1 \end{pmatrix} \cdot L_P \end{aligned} \tag{9}$$

where $\mathbf{c}$ is a bidimensional basis function, which discrete form is a $(n_{dof} \times 1)$ vector with n_{dof} the number of degree of freedom. In consequence, the vectors $\mathbf{0}$ in Eq. (9) have the appropriate number of elements to fulfill the $\mathbf{c}$ discrete vector size. Here, function L_p depends on the p-th variable associated to the material property of node/parameter p. This spatial format of the material property/internal variable is forwardly integrated into the weak form of the boundary value problem. A multidimensional PGD procedure is implemented for the microscale problem as described in [16], where an additive split of the displacement field is introduced [4, 30, 16], which writes:

$$\mathbf{u} = \mathbf{u}^M + \mathbf{u}^m \tag{10}$$

being $\mathbf{u}^M$ and $\mathbf{u}^m$ the macroscale and microscale related variables of the displacement field, respectively. The functional space of $\mathbf{u}^M$ is denoted by $\mathfrak{L}^{\mathfrak{M}}$ and the one of $\mathbf{u}^m$ by $\mathfrak{L}^{\mathfrak{m}}$. The direct sum of these spaces is specified as $\mathfrak{L} = \mathfrak{L}^{\mathfrak{M}} \bigoplus \mathfrak{L}^{\mathfrak{m}}$. The test function, $\boldsymbol{\upsilon}$, is similarly decomposed into micro and macro components $\boldsymbol{\upsilon}^M$ and $\boldsymbol{\upsilon}^m$.

$$\boldsymbol{\upsilon}(x) = \boldsymbol{\upsilon}^M(x) + \boldsymbol{\upsilon}^m(x) \tag{11}$$

Then the weak form of the microscale parametrized problem is written as:

$$\int_\Omega (\delta\boldsymbol{\varepsilon}^M + \delta\boldsymbol{\varepsilon}^m)^T \mathbf{D}(\boldsymbol{\varepsilon}, \boldsymbol{\kappa})(\boldsymbol{\varepsilon}^M + \boldsymbol{\varepsilon}^m) d\Omega = \int_\Omega (\boldsymbol{\upsilon}^M + \boldsymbol{\upsilon}^m)^T \mathbf{f}\, d\Omega \tag{12}$$

where $\mathbf{D}$ represents the matrix of elasticity, $\boldsymbol{\varepsilon}$ and $\delta\boldsymbol{\varepsilon}$ are the actual strain vector and the virtual strain associated to the test function $\mathbf{v}$, respectively. Here the variable to be parametrized is the microscale displacement $\mathbf{u}^m$, which will be solved for homogeneous boundary condition, hence, $\mathbf{u}^M$ should approximate the solution $\mathbf{u}$ with sufficient accuracy at microscale domain $\partial\Omega_m$. The $\mathbf{u}^M$ is written in a separated format as:

$$\mathbf{u}^M = \sum_{s=1}^{S} \mathbf{a}_s^M(\mathbf{x}^m) \prod_{k=1}^{D} G_s^{k^M}(z_k) \prod_{p=1}^{P} H_s^{p^M}(e_p) \tag{13}$$

A predefined approximation of the boundary displacement for the microscale domain had to be established, through which the number of variables related to boundary conditions ($G^k(z_k)$ for $k = 1, \ldots, D$) is defined. Considering a $2D$ voxel domain for the microscale model and a linear boundary

approximation, then 8 variables are needed, representing the displacement in x and y directions for each vertex node. Consequently, the macroscale displacement field in the RVE can be defined by the standard bilinear interpolation, although, more complex interpolations may be used.

$$\mathbf{u}^M = (1-x^m)(1-y^m)\mathbf{u}_1^M + x^m(1-y^m)\mathbf{u}_2^M + x^m y^m \mathbf{u}_3^M + (1-x^m)y^m\mathbf{u}_4^M \tag{14}$$

Note that (14) already has a separated structure, however, for non trivial separated function, a Singular Value Decomposition (SVD) [23] or Parallel Factors Decomposition (PARAFAC) [39] procedure can be implemented to obtain a separated format of the macroscale function. Reader can refer to [16] for a detailed description of boundary conditions parametrization in a separated format.

The numerical scheme to solve the problem consists in the iterative procedure proposed in [21, 27]. Let us assume I terms of the finite sum for the u^m variable already computed, and the current approximation is not sufficiently accurate (the convergence check is not fulfilled) [21, 23, 16], a new functional product $I+1$ is added to the finite sum. In this "enrichment stage" [21, 23] the approximation of u^m can then be written as follows:

$$\mathbf{u}^m = \sum_{i=1}^{I} \mathbf{a}_i^m(\mathbf{x}) \prod_{k=1}^{D} G_i^{k^m}(z_k) \prod_{p=1}^{P} H_i^{p^m}(e_p) + \mathbf{r}(\mathbf{x}) \prod_{k=1}^{D} M^k(z_k) \prod_{p=1}^{P} O^p(e_p) \tag{15}$$

For example, the microscale strain vector in terms of the displacement field approximation (15) for a 2-D case in the standard finite element framework, writes:

$$\begin{aligned} \boldsymbol{\varepsilon} = \begin{pmatrix} \sum_{i=1}^{I} \frac{\partial a_x^{i^m}}{\partial x} \cdot ORV + \frac{\partial r_x}{\partial x} \cdot NRV \\ \sum_{i=1}^{I} \frac{\partial a_y^{i^m}}{\partial y} \cdot ORV + \frac{\partial r_y}{\partial y} \cdot NRV \\ \sum_{i=1}^{I} (\frac{\partial a_x^{i^m}}{\partial y} + \frac{\partial a_y^{i^m}}{\partial x}) \cdot ORV + (\frac{\partial r_x}{\partial y}) + \frac{\partial r_y}{\partial x}) \cdot NRV \end{pmatrix} = \\ = \sum_{i=1}^{I} \mathbf{B}\mathbf{a}^{i^m} \cdot ORV + \mathbf{B}\mathbf{r} \cdot NRV \end{aligned} \tag{16}$$

where,

$$
\begin{aligned}
ORV &= \prod_{k=1}^{D} G_i^{k^m}(z_k) \prod_{p=1}^{P} H_i^{p^m}(e_p) \\
NRV &= \prod_{k=1}^{D} M^k(z_k) \prod_{p=1}^{P} O^p(e_p)
\end{aligned}
\tag{17}
$$

The strain related to the macroscale is fixed when computing $\mathbf{u}^m$, therefore, the associated test function $\boldsymbol{\upsilon}^M$ and $\delta\boldsymbol{\varepsilon}^M$ vanish, while $\boldsymbol{\upsilon}^m$ can be expressed as:

$$
\begin{aligned}
\boldsymbol{\upsilon}^m = \mathbf{r}^* \prod_{k=1}^{D} M^k(z_k) \prod_{p=1}^{P} O^p(e_p) + \mathbf{r} \prod_{k=2}^{D} M^{1^*}(z_1) M^k(z_k) \prod_{p=1}^{P} O^p(e_p) + \cdots \\
\cdots + \mathbf{r} \prod_{k=1}^{D-1} M^k(z_k)(z_k) M^{D^*}(z_D) \prod_{p=1}^{P} O^p(e_p) + \mathbf{r} \prod_{k=1}^{D} M^k(z_k) \prod_{p=2}^{P} O^{1^*}(e_1) O^p(e_p) + \\
\cdots + \mathbf{r} \prod_{k=1}^{D} M^k(z_k) \prod_{p=1}^{P-1} O^p(e_p) O^{P^*}(e_P)
\end{aligned}
\tag{18}
$$

the same procedure of $\boldsymbol{\upsilon}^m$ is followed for $\delta\boldsymbol{\varepsilon}^m$ definition.

Considering the stiffness matrix decomposition and a finite element formulation, the alternate direction algorithm starts computing function $\mathbf{r}(\mathbf{x}^m)$ assuming M^k and O^p known, so M^{k^*} and O^{p^*} vanish. Introducing equations (6), (8), (13), (15), (16) and (18) in the weak form (12) gives:

$$\int_{\Omega} \mathbf{r}^* \mathbf{B}^T \prod_{k=1}^{D} M^k(z_k) \prod_{p=1}^{P} O^p(e_p) \big(\mathbf{D} \sum_{q=1}^{Q} \hat{\mathbf{c}}_q(\mathbf{x}) L_q(e_q)\big) \cdot$$
$$\cdot \big[\sum_{s=1}^{S} \mathbf{Ba}_s^M(\mathbf{x}) \prod_{k=1}^{D} G_s^{k^M}(z_k) \prod_{p=1}^{P} H_s^{p^M}(e_p) +$$
$$+ \sum_{i=1}^{I} \mathbf{Ba}_i^m(\mathbf{x}) \prod_{k=1}^{D} G_i^{k^m}(z_k) \prod_{p=1}^{P} H_i^{p^m}(e_p) + \mathbf{Br}(\mathbf{x}) \prod_{k=1}^{D} M^k(z_k) \prod_{p=1}^{P} O^p(e_p) \big] d\Omega =$$
$$= \int_{\Omega} \mathbf{r}^* \mathbf{N}^T \prod_{k=1}^{D} M^k(z_k) \prod_{p=1}^{P} O^p(e_p) \mathbf{f} d\Omega \tag{19}$$

Rearranging (19) and separating the microscale spatial integral from the rest, the following expression arises, the linear system based in Eq. (19) can be explicitly written as:

$$\mathbf{K}_r \cdot \mathbf{r} = \mathbf{p}_r - \mathbf{t}_1 - \mathbf{t}_2 \tag{20}$$

where,

$$\mathbf{K}_r = \sum_{q=1}^{Q} \mathbf{r}^* \big[\int_{\Omega_{sp}^m} \mathbf{B}^T \mathbf{D} \mathbf{B} \hat{\mathbf{c}}_q(\mathbf{x}) d\Omega_{sp}^m \big] \mathbf{r} \prod_{k=1}^{D} \int_{\Omega_k} M^k(z_k) M^k(z_k) d\Omega_k \cdot$$
$$\cdot \prod_{p=1}^{P} \int_{\Omega_p} O^p(e_p) O^p(e_p) L_q(e_q) d\Omega_p$$

$$\mathbf{t}_1 = \sum_{q=1}^{Q} \sum_{s=1}^{S} \mathbf{r}^* \big[\int_{\Omega_{sp}^m} \mathbf{B}^T \mathbf{D} \mathbf{B} \hat{\mathbf{c}}_q(\mathbf{x}) d\Omega_{sp}^m \big] \mathbf{a}_s^M \prod_{k=1}^{D} \int_{\Omega_k} M^k(z_k) G_s^{k^M}(z_k) d\Omega_k \cdot$$
$$\cdot \prod_{p=1}^{P} \int_{\Omega_p} O^p(e_p) H_s^{p^M}(e_p) L_q(e_q) d\Omega_p$$

$$\mathbf{t}_2 = \sum_{q=1}^{Q}\sum_{i=1}^{I}\mathbf{r}^*\big[\int_{\Omega_{sp}^m}\mathbf{B}^T\mathbf{D}\mathbf{B}\hat{\mathbf{c}}_q(\mathbf{x})d\Omega_{sp}^m\big]\mathbf{a}_i^m\ \prod_{k=1}^{D}\int_{\Omega_k}M^k(z_k)G_s^{k^m}(z_k)d\Omega_k\cdot$$
$$\cdot\prod_{p=1}^{P}\int_{\Omega_p}O^p(e_p)H_i^{p^m}(e_p)L_q(e_q)d\Omega_p$$

$$\mathbf{p}_r = \mathbf{r}^*\big[\int_{\Omega_{sp}^m}\mathbf{N}^T\mathbf{N}d\Omega_{sp}^m\big]\mathbf{f}^{sp}(\mathbf{x}^m)\ \prod_{k=1}^{D}\int_{\Omega_k}M^k(z_k)f_k(z_k)d\Omega_k\cdot$$
$$\cdot\prod_{p=1}^{P}\int_{\Omega_p}O^p(e_p)f_p(e_p)d\Omega_p$$

Note that the body force term is written in a separated representation $f = f^{sp}(\mathbf{x}^m)\prod_{k=1}^{D}f_k(z_k)\prod_{p=1}^{P}f_p(e_p)$. Note also that the integral $\int_{\Omega_{sp}^m}\mathbf{B}^T\mathbf{D}\mathbf{B}d\Omega_{sp}^m$ in the latter equation is the standard stiffness matrix for the macroscale finite element.

This procedure is repeated for the rest of dimensions, and stops when each of these vectors reach a fix value, see Algorithm 1. Notice that complex microscale domain (RVE) can be handle by this formulation because no separation of the microscale coordinate is done.

Once the parametrization of the displacement field is obtained for the microscale model, the macroscale problem can be then solved by an explicit or implicit procedure. For example, recalling the Newton Raphson (N-R) implicit procedure, where we assumed solved the state at t and wish to update state to $(t+\triangle t)$ of the problem. For i^{th} N-R iteration displacement increment is defined as:

$$\mathbf{K}(\mathbf{u}_i^{t+\triangle t})\Delta(\mathbf{u}_{i+1}) = -\Psi(\mathbf{u}_i^{t+\triangle t}) \tag{21}$$

where $\mathbf{K}$ is the tangent stiffness matrix. The N-R starts with an initial guess of $\mathbf{u}_i^{t+\triangle t}$ for the macroscale problem, from which a distribution of the material property/internal variable $E(\mathbf{u}_i^{t+\triangle t})$ is computed by its governing equation with a microscale model resolution. The internal force and tangent modulus

Algorithm 1 Microscale Step Algorithm

while $Res > TOL$ **do**
  Initialize $\mathbf{r}_k \quad k = 1, \ldots, D$ (with $\mathbf{r}_k$ initial k-th parameter function of the new sum.)
  while $e\_enr_k > TOL_k$ **do**
    for $k = 1 : D$ **do**
      Compute $\mathbf{r}_k^n$
      Compute e_enr_k
    end for
    Set $\mathbf{r}_k = \mathbf{r}_k^n$
    Set $n = n + 1$
  end while
  Set $\mathbf{f}_k^i = \mathbf{r}_k$
  Compute Res
  Set $i = i + 1$
end while

matrix are obtained for each macroscale element from the displacement field distribution obtained by particularizing the "off-line" results for the elastic property/internal variable distribution and displacement boundary conditions as shown in Appendix A. Note that no further boundary value problem is needed for each RVE as in traditional multilevel finite element (FE^2). A scheme of this multiscale strategy is presented in Fig. 1.

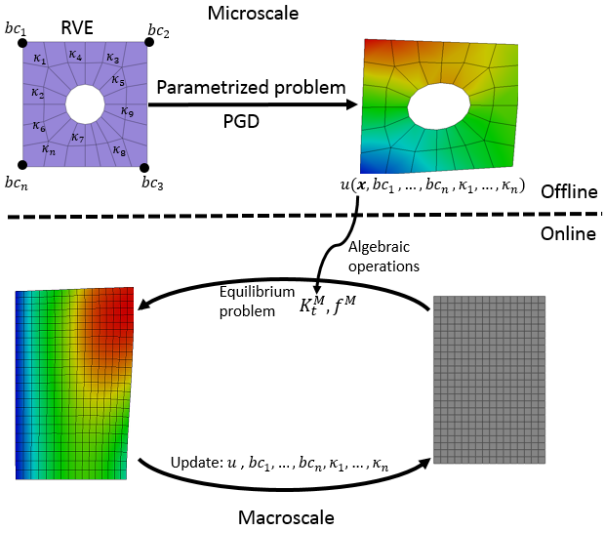

Figure 1: Multiscale strategy scheme: Micro-step Uncoupling Equilibrium and Evolution Equations.

3.2. 2nd Strategy: Microscale parametrization within the macroscale problem

Another way to deal with material non-linearities, thought to alleviate the parametrized microscale problem, is by incorporating the microscale parametrized problem into the macroscale incremental problem. This can be achieved by building and solving by PGD a parametrized microscale problem for the actual material property/internal variable distribution associated to the actual macroscale load increment. Then, the microscale displacement distribution over the RVE is parametrized only with respect to the microscale coordinates, boundary conditions approximation and macroscale element. The scheme followed in this strategy is depicted in Fig. 2.

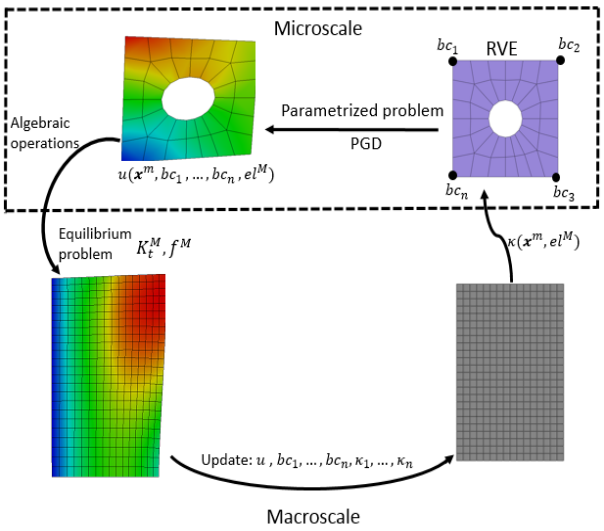

Figure 2: Multiscale strategy scheme: Microscale parametrization within the macroscale problem.

The material property/internal variable is now approximated as a sum of separated functions describing in each one the microscale spatial dependency and the corresponding macroscale element, this approximation can be written as,

$$E(\mathbf{x}^m, el^M) = \sum_{p=1}^{P} \mathbf{c}_p(\mathbf{x}^m) H_p(el^M) \tag{22}$$

where, $\mathbf{c}_p(\mathbf{x}^m)$ and $H_p(el^M)$ are the p-th function of the approximation that depend on the microscale coordinate and the macroscale element (el^M) variable, respectively. Here, the parametrization is solved for the total number of macroscale elements. For which a separated representation of the distribution can be derived through SVD [23].

The proposed methodology can be labeled as $FE - PGD$, where a finite element approach is implemented to solve the macroscale problem and a PGD parametrized microscale problem is solved for each time increment. The "off-line" step is suppressed for this methodology, since the reduced parametrized microscale problem is solved directly along the process. The advantage over the traditional multilevel finite element approach FE^2 relies

in substituting the different boundary condition problem for each RVE by a multiparametric RVE problem solved by PGD. Each stiffness matrix and internal forces vector is computed by means of algebraic operations particularizing the parametrized problem results as resumed in Appendix A.

As in the first strategy, the displacement field approximation is again split into a macro and micro displacement and represented in a separated format as,

$$\triangle \mathbf{u} = \triangle \mathbf{u}^M + \triangle \mathbf{u}^m \tag{23}$$

$$\triangle \mathbf{u}^M = \sum_{s=1}^{S} \mathbf{a}_s^M(\mathbf{x}^M) S_s^M(el^M) \prod_{k=1}^{D} G_s^{k^M}(z_k) \tag{24}$$

$$\triangle \mathbf{u}^m = \sum_{i=1}^{I} \mathbf{a}_i^m(\mathbf{x}^m) S_i^m(el^M) \prod_{k=1}^{D} G_i^{k^m}(z_k) \tag{25}$$

where, $G_i^k(z_k)$ the k-th variable, D is assumed to be the number of variables associated to the Dirichlet boundary condition approximation [16] and S represents the number of terms for the predefined displacement approximation defined by the macroscale displacement term $\triangle \mathbf{u}^M$. The macroscale displacement term can be implemented as in the previous strategy. For each time increment of the macroscale problem, a parametrized microscale boundary value problem for the spatial distribution of the material property/internal variable given by (22) is solved. Recalling the numerical scheme to solve the parametrized problem through PGD, and assuming I terms of the finite sum for the u^m variable already computed, and the current approximation is not sufficiently accurate, a new functional product $I+1$ is added to the finite sum. Then u^m can then be written as follows:

$$\triangle \mathbf{u}^m = \sum_{i=1}^{I} \mathbf{a}_i^m(\mathbf{x}^m) S_i^m(el^M) \prod_{k=1}^{D} G_i^{k^m}(z_k) + \mathbf{r}(\mathbf{x}^m) M(el^M) \prod_{k=1}^{D} O^k(z_k) \tag{26}$$

The weak form of the parametrized problem (12) after introducing the displacement, test functions (as shown in (18)) and material property (22)

approximations can be expressed as:

$$\int_{\Omega} \mathbf{r}^{*}\mathbf{B}^{T} M(el^{M}) \prod_{k=1}^{D} O^{k}(z_k)\big(\mathbf{D}\sum_{p=1}^{P}\mathbf{c}_p(\mathbf{x}^m)H_p(el^M)\big)\cdot$$
$$\cdot\,\big[\sum_{s=1}^{S}\mathbf{a}_s^M(\mathbf{x}^M)S_s^M(el^M)\prod_{k=1}^{D}G_s^{k^M}(z_k)+\sum_{i=1}^{I}\mathbf{a}_i^m(\mathbf{x}^m)S_i^m(el^M)\prod_{k=1}^{D}G_i^{k^m}(z_k)+$$
$$+\,\mathbf{r}(\mathbf{x}^m)M(el^M)\prod_{k=1}^{D}O^k(z_k)\big]d\Omega=\int_{\Omega}\mathbf{r}^{*}\mathbf{N}^{T}\prod_{k=1}^{D}M^k(z_k)\prod_{p=1}^{P}O^p(e_p)\mathbf{f}d\Omega \tag{27}$$

The fix point procedure to solve the problem as described in section 3.1 is implemented. An incremental explicit multiscale procedure for the FE-PGD formulation is summarized in Algorithm 2.

Algorithm 2 Incremental Explicit Multiscale Procedure for the FE-PGD Formulation

1: Initialize E (Elastic modulus/Internal variable distribution)
2: **for** $\triangle t = 1 \rightarrow n_{inc}$ **do**
3: Compute separated expression for $E(\mathbf{x}^m, el^M)$
4: Parametrized microscale problem (PGD) with $E(\mathbf{x}^m, el^M)$
5: Compute $\triangle\mathbf{p}_{ext}$ (Macroscale nodal external forces vector)
6: Initialize $\mathbf{u}$ (Nodal displacement vector for macroscale problem)
7: **for** $c = 1 \rightarrow el^M$ **do**
8: Compute microdisplacement field for macroelement c by particularizing the PGD step
9: Compute $\triangle\mathbf{p}_{int}^c$ (Microscale loop)
10: Compute $\mathbf{K}^c$ (Microscale loop)
11: **end for**
12: Assemble $\triangle\mathbf{p}_{int}$ and $\mathbf{K}$
13: Compute displacement increment $\mathbf{K}\triangle\mathbf{u} = \triangle\mathbf{p}_{ext} - \triangle\mathbf{p}_{int}$
14: Set $\mathbf{u} = \mathbf{u} + \triangle\mathbf{u}$
15: Update E by the governing equation.
16: **end for**

4. Numerical Example: Non-Linear 2-D Example with Rate-Dependent Damage Model.

An example to check the performance of both multiscale strategies for non-linear problems has been analyzed. A multiscale problem with periodic voids and boundary conditions described in Fig. 3 is analyzed for a rate-dependent damage model. A load in x direction of $1300N$ over one edge is applied in a total time of $9.4s$. An incremental scheme has been applied for the analysis with a time increment of $0.2s$. The macroscale problem with a rectangular geometry $x \in [0, 4mm]$ and $y \in [0, 3mm]$ is then computed by the multiscale procedures here proposed with 192 regular quadrilateral elements of side $0.25mm$, which represent the problem RVE. The parametrized RVE for this problem was discretized with 39 linear quadrilateral elements and 56 nodes. Results were compared with a traditional FE model discretized by 8425 linear quadrilateral elements, which represents the discretization of the problem if the RVE discretization is used.

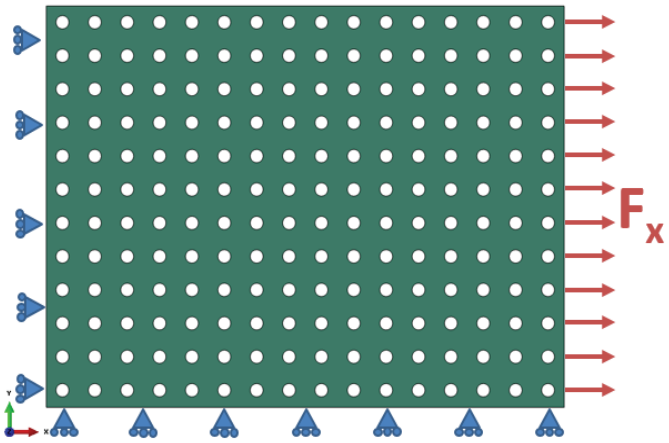

Figure 3: Boundary conditions and edge force for the periodic voids 2-D example.

For instance, let us consider a rate-dependent isotropic damage law. The damage model employs irreversible thermodynamics and the internal state variables theory. To introduce the scalar damage behavior, let us consider the effective stress concept through equilibrium considerations, whereby

$$\boldsymbol{\sigma}(\boldsymbol{\varepsilon}, \omega) = [1 - \omega]\boldsymbol{\sigma}_0(\boldsymbol{\varepsilon}) = [1 - w]\mathbf{D}_0\boldsymbol{\varepsilon} \tag{28}$$

where, $\boldsymbol{\sigma}$ and $\boldsymbol{\varepsilon}$ represent the Cauchy stress and strain tensors, respectively. The subscript $(\bullet)_0$ represents magnitudes of an undamaged (virgin) material and ω denotes the isotropic damage parameter. The function $G(\bar{Y})$ which characterizes the damage process in the material is chosen as an exponential function, which described most damage models found in literature, such as the three-parameter Weibull distribution [31] which expression enables it to capture a wide range of material behaviors [32]. This function reads

$$G(\bar{Y}) = 1 - exp\left[-\left(\frac{\bar{Y}(\boldsymbol{\varepsilon})}{p_1}\right)^{p_2}\right] \tag{29}$$

where, p_1 and p_2 are non-dimensional scale and shape parameter, respectively. Here, $\bar{Y}(\boldsymbol{\varepsilon})$ denotes the thermodynamic force (damage energy release rate)

$$\bar{Y}(\boldsymbol{\varepsilon}) = \frac{1}{2}\boldsymbol{\varepsilon}\mathbf{D}_f\boldsymbol{\varepsilon} \tag{30}$$

$\mathbf{D}_f$ is the elastic stiffness of micro-material .

The damage evolution model taken as example is based on the one proposed in [33] for particulate composite materials and known as viscous damage model [36, 37]. In particular, the evolution equation for $\dot{w}$ that governs the visco-damage behavior assuming a linear viscous damage mechanism can be written as:

$$\dot{\omega} = \mu g \tag{31}$$

where, μ denotes the damage viscosity coefficient. The state of damage in the material is governed by the following criterion:

$$g(\bar{Y}, \chi) = G(\bar{Y}) - \chi^t \leq 0 \quad t \subset \mathbb{R}^+ \tag{32}$$

where χ^t denotes the softening parameter usually set as χ^0=0 [33], and will be considered for this work as $\chi^t = \omega$.

To integrate the evolution equation to solve the damage problem in the traditional FEM framework, the implicit backward Euler integration scheme has be employed. Thus the equations of evolution are solved incrementally over a sequence of given time steps $[t_n, t_{n+1}] \subset \mathbb{R}^+$, $n = 0, 1, 2, \ldots$ with initial conditions $\{\boldsymbol{\sigma}, \omega\}|_{t=t_n} = \{\boldsymbol{\sigma}_n, \omega_n\}$. The time step is given by $\triangle t = t_{n+1} - t_n$.

The rate-dependent damage integration into the problem is described in Algorithm 3.

Algorithm 3 Rate-dependent damage integration algorithm.

1: Compute $\bar{Y}_{n+1} = \frac{1}{2}\boldsymbol{\varepsilon}_{n+1}\mathbf{D}_f\boldsymbol{\varepsilon}_{n+1}$
2: Check $g = G(\bar{Y}_{n+1}) - \omega_n > 0$?
   No $\rightarrow$ no damage within this time step EXIT
   Yes $\rightarrow$ rate-dependent damage loading CONTINUE
3: Compute ω_{n+1}
   $\omega_{n+1} = \omega_n(1 - \triangle t\mu) + \triangle t\mu G(\bar{Y}_{n+1})$
4: Update stress
   $\boldsymbol{\sigma}^0_{n+1} = \mathbf{D}_0\boldsymbol{\varepsilon}_{n+1}$
   $\boldsymbol{\sigma}_{n+1} = (1 - \omega_{n+1})\boldsymbol{\sigma}^0_{n+1}$

If an implicit scheme is used to solve this non-linear problem, a consistent linearization is important if one wants to keep quadratic rate of convergence, when Newton's type algorithm is employed. The linearized term associated with the damage law for computing the tangent elastic matrix is given by

$$\frac{\partial \mathbf{D}}{\partial \mathbf{u}} = \frac{\partial[(1-\omega)\mathbf{D}_0]}{\partial \mathbf{u}} = \frac{\partial G(\bar{Y})}{\partial \bar{Y}}\frac{\partial \bar{Y}}{\partial \boldsymbol{\varepsilon}}\frac{\partial \boldsymbol{\varepsilon}}{\partial \mathbf{u}}\mathbf{D}_0 \tag{33}$$

where for the incremental scheme

$$\frac{\partial G(\bar{Y})}{\partial \bar{Y}_{n+1}} = \frac{p_2 \triangle t\mu}{p_1} exp\left[-\left(\frac{\bar{Y}_{n+1}}{p_1}\right)^{p_2}\right]\left(\frac{\bar{Y}_{n+1}}{p_1}\right)^{p_2-1} \tag{34}$$

4.1. 1^{st} Strategy

For the multiscale procedure based on the uncoupled strategy, the parametrized microscale problem is built considering internal variables associated to each node of the microscale mesh as an extra variable. Taking as example the rate-dependent isotropic damage problem presented before, the first step to construct the microscale parametrized model is to define the desired parameters that will be considered extra variables of the original problem and which will define the dimension of the problem. The total dimensions of

the parametrized problem is 65, represented by the micro spatial coordinates (1), Dirichlet boundary condition approximation in both directions (8) and isotropic damage value in each node(56). Therefore, the displacement field can be obtained particularizing the "off-line" step results for a specific displacement boundary condition and nodal distribution of internal variable.

For the present example, the predefined range and discretization of the scalar damage parameter associated to each node were set to $\omega = [0, 0.8]$ and $\triangle\omega = 0.02$, respectively. The range and discretization considered for the variables associated to the boundary condition are shown in Table 1.

Independent Variable	Variable Interval [**mm**]	Discretization Size [**mm**]
$u_2^x \;\; u_3^x \;\; u_4^x$	[−0.05,0.05]	0.001
$u_2^y \;\; u_3^y \;\; u_4^y$	[−0.05,0.05]	0.001

Table 1: Boundary condition variables ranges and element size for the rate-independent damage model analyzed in the periodic void problem.

For the microscale solution validation, results of the displacement field approximation were compared to those obtained by an incremental explicit FEA. Two states of deformation were chosen for validation as shown in Table 2 and considering relative L_2 norm errors as

$$err = \sqrt{\frac{\sum_{i=1}^{n}(df_i)^2}{\sum_{i=1}^{n}(u_i^t)^2}} \tag{35}$$

where *df* is the difference between the standard FE with a very fine discretization and the numerical results.

Case	u_2^x [mm]	u_3^x [mm]	u_4^x [mm]	u_2^y [mm]	u_3^y [mm]	u_4^y [mm]
1	0.001	0.0094	0.004	0.003	-0.005	-0.0045
2	0.01	-0.005	0.0	0.0	0.01	0.0034

Table 2: Independent variables values for the microscale step verification for each case in the example with the rate-dependent damage material model analyzed with the uncoupled microscale problem procedure.

Due to the dimensionality of the problem a high number of terms for the approximation were needed for convergence of the PGD technique. In Fig. 4(a) the L_2 relative norm errors (35) of the displacement vector against the number of terms in the approximation were plotted for the boundary condition case 1 shown in Table 2, furthermore, the scalar damage nodal distribution plotted is shown in Fig. 4(b). It can be observed how the convergence curve in Fig. 4(a) shows a quasi stationarity behaviour from a certain number of terms. This demonstrates that there is a limit of terms for the approximation from which low or no improvements of the solution is achieved. The latter limit depends on parameter discretization in the parametrized problem and on the separability of the solution. Furthermore, introducing modes computed via Proper Orthogonal Decomposition (POD) [35] to define the distribution of the isotropic damage could be advantageous, not only for ensuring independency of the distribution approximation, but also the number of parameters for the isotropic damage distribution approximation would be lower. This has been recently applied to initial conditions approximations for dynamic problems as shown in [34], where a solution has been introduced by an off-line/on-line strategy in which a reduced-order basis, obtained via POD, is employed, thus guaranteeing the parametrization of the space of initial conditions with a minimum of variables. Even with this efficient approach for the initial conditions, the number of parameters usually reaches some tens for spatial 3-D problems.

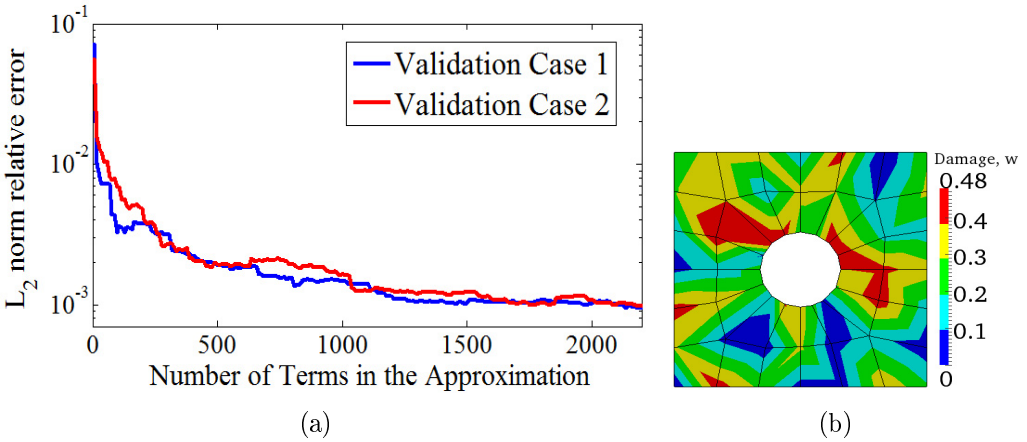

(a) (b)

Figure 4: (a)L_2 relative norm errors (35) compared to a standard FE of the incremental displacement vector against the number of terms in the approximation for the microscale parametrized problem of 65 dimensions (b) Damage internal variable distribution over the RVE for the parametrization problem validation.

The displacement field in both directions (Figs. 5(a) and 5(c)) over the microscale model for the boundary displacement case 1 (Table 2) and the random isotropic damage distribution shown in Fig. 4(b) were compared to the results obtained through an explicit FE analysis with the same increment size. L_2 norm relative errors (35) of 1.7×10^{-3} and 2.5×10^{-3} were computed for x and y displacements, respectively. Relative errors (36) between both results were plotted in Figs. 5(b) and 5(d) for directions x and y, respectively. The relative error for the $i-th$ node is computed as,

$$df_i = \frac{|u_i^{FE} - u_i^{PGD}|}{|u_i^{FE}|} \tag{36}$$

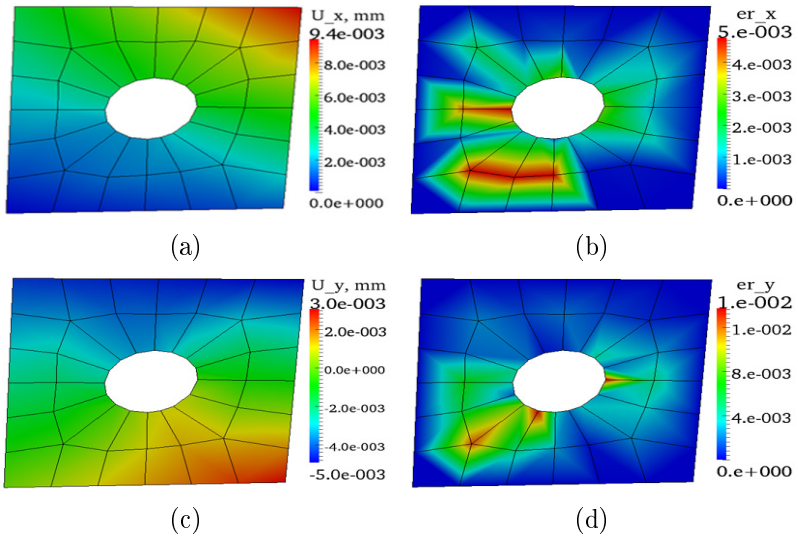

Figure 5: Microscale results for the rate-dependent damage model for case of deformation 1 (Table 2) with a isotropic damage distribution plotted in Fig. 4(b). (a) and (c) displacement field distribution in x and y directions, respectively. (b) and (c) relative displacement error distribution compared to the standard FE analysis under the same conditions in x and y directions, respectively.

Computer time for the "off-line" microscale step for the 65-dimensional problem is plotted vs. the number of terms for the approximation in Fig. 6. Also a 101-dimensional micro problem parametrization was computed with 92 extra variables associated to each node in a refined RVE discretization. The corresponding computer time is also shown in Fig. 6. The post-processing time for particularizing the displacement field approximation over the RVE for a predefined displacement boundary condition and damage distribution is around $0.012s$ for a 2600-terms approximation, which represents the 8% of the computer time ($0.15s$) needed for solving the micro problem through the standard FE procedure.

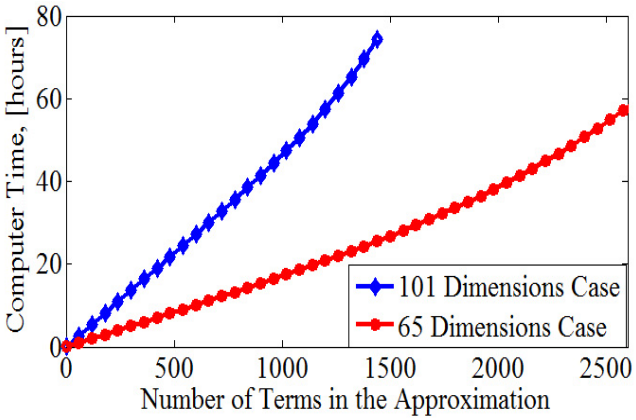

Figure 6: Computer time for the "off-line" microscale step vs. the number of terms for the approximation for a 65 and 101 dimensions problem.

The macroscale problem is then solved through an explicit scheme using the "off-line" parametrized results. The internal variable evolution was computed by the traditional implicit backward Euler scheme. L_2 norm relative errors (35) at the macroscale displacement field for x and y directions were 3.6×10^{-3} and 5.8×10^{-3}, respectively. The localized microscale displacement field over the macroscale model was compared to that computed through the incremental explicit FE procedure, relative errors results are shown in Fig. 7. Moreover, the resultant isotropic damage distribution over the geometry at the microscale level for the final state of deformation was computed and the associated relative error with respect to the damage distribution through the standard FE analysis is shown in Fig. 7(c), where a L_2 norm relative error of 0.041 was obtained. As expected, higher deviations in the isotropic damage distribution was observed, due to the non-linear dependency on the derivative of the displacement field as shown in (30).

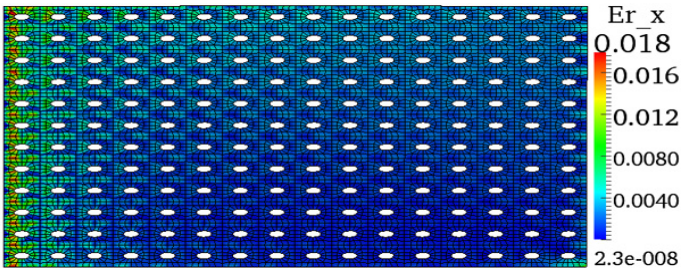

(a)

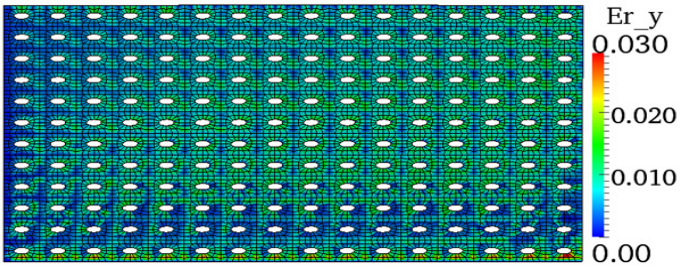

(b)

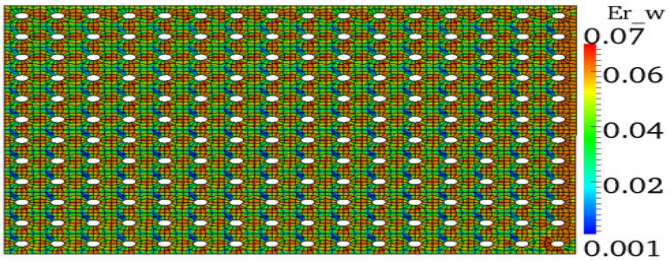

(c)

Figure 7: Relative error distribution in displacements between the results obtained through the multiscale approach by the uncoupled problem scheme and with the standard FE analysis with 8425 elements for x (a) and y (b) directions. (c) Isotropic damage relative error distribution compared to the traditional explicit FE analysis.

Computer time of the macroscale problem was compared to that obtained with a traditional FE approach. For this, the FE analysis have been implemented within MATLAB for a fair comparison. Macroscale step took about $298s$, validating the strong reduction got when compared to the $1100s$ required to solve the problem with a standard FE procedure and the corresponding much higher computer memory requirement.

4.2. 2^{nd} Strategy

Again the problem described in Fig. 3 has been analyzed for the rate-dependent damage model presented before. Firstly, the same load condition and total time of $1300N$ and $9.4s$, respectively, were used for comparison purposes. An incremental scheme has been applied with a time increment of $0.2s$.

Displacement fields in the macroscale mesh were compared to those obtained by the traditional FE analysis, observing a L_2 relative norm error (35) of 2.2×10^{-3} and 3.3×10^{-3} for the x and y directions, respectively. Furthermore, the localization of the microscale displacement field was computed for all the macroscale elements and compared to the detailed FE analysis. The relative errors (36) for both directions have been plotted in Figs. 8(a) and 8(b), and the same error for the isotropic damage distribution compared to that obtained through the standard FE analysis was represented in Fig. 8(c). A second case has been checked changing the time increment to $0.5s$ and keeping the rest of parameters. For this case, the L_2 relative norm errors (35) for the x and y direction were 3.5×10^{-3} and 8.3×10^{-3}, respectively.

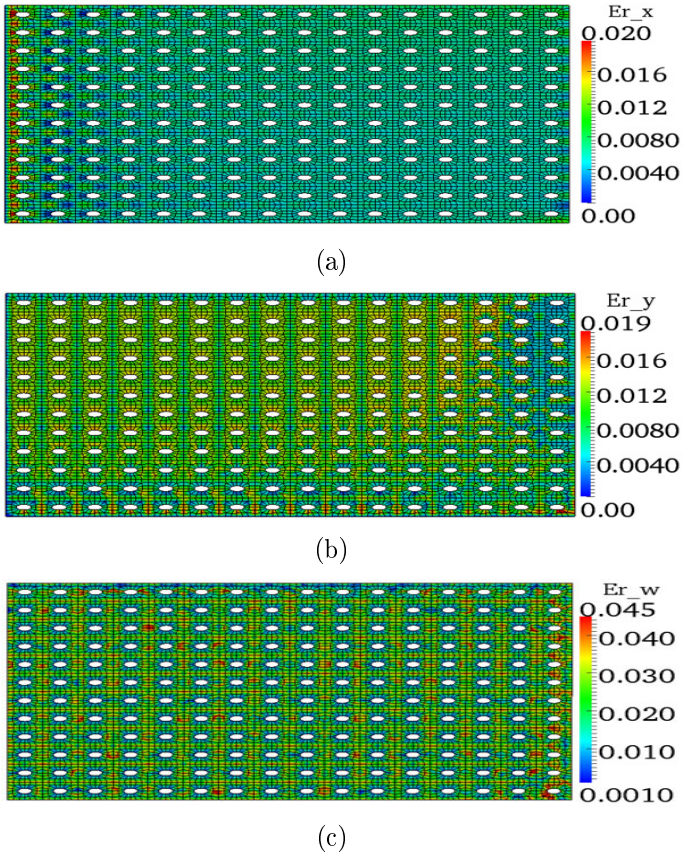

Figure 8: Relative error distribution in displacements between the results obtained through the multiscale approach by the FE-PGD scheme and with the standard FE analysis with 8425 elements for x (a) and y (b) directions. (c) Isotropic damage relative error distribution compared to the traditional explicit FE analysis.

Localized stress distribution for the periodic voids example obtained through the multiscale approach by the FE-PGD scheme (with a time increment of $0.2s$) for x and y directions are plotted in Figs. 9(a) and 9(b), respectively. In addition, the stress distribution obtained by the standard FE analysis with 8425 elements for x (c) and y (d) directions are shown in Figs. 9(c) and 9(d), respectively. L_2 relative norm error (35) of 3.5×10^{-2} and 4.9×10^{-2} for the stress variable in x and y directions have been computed, respectively.

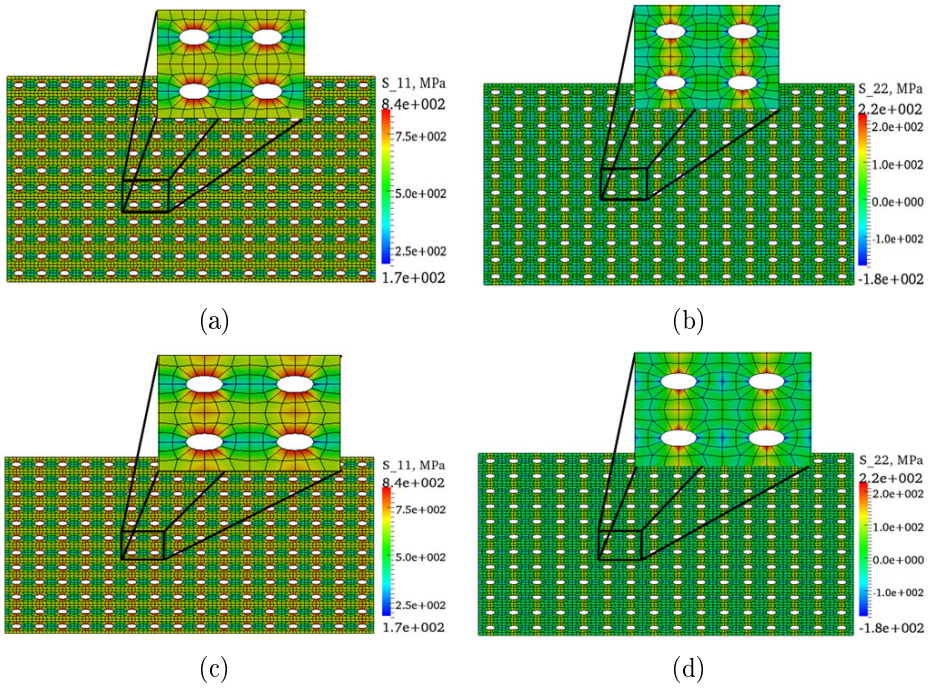

Figure 9: Localized stress distribution for the periodic voids example obtained through the multiscale approach by the FE-PGD scheme for x (a) and y (b) directions and stress distribution obtained by the standard FE analysis with 8425 elements for x (c) and y (d) directions.

Computer time of the macroscale problem was again compared to that obtained with the FE approach. Macroscale step took about $710s$, that is again lower than the time for a traditional FE incremental scheme under the same conditions $1100s$. The microscale parametrized step within each increment in the macroscale problem was about $10s$ to achieve a mean of 50 terms in each incremental displacement field approximation. The computer time comparison becomes more representative when a more discretized microscale model is used. For this, the microscale model was refined from 39 to 92 quadrilateral elements, and under the same conditions a total time of $1140s$ for the macroscale problem was achieved. Meanwhile, the detailed discretization FE analysis for the same microscale elements size results in 12864 elements, for which a total time of $2520s$ and a considerable higher computer memory was required.

5. Conclusions

A multiscale formulation for problems with material non-linearities in small deformation regimes has been presented. Two different options based on parametrized microscale models solved by PGD have been applied to a problem with a rate-dependent isotropic damage model. First, a procedure where the problem is solved by uncoupling the equilibrium equation and the state variable expression has been explored. For this, a predefined spatial distribution approximation of the state variable is considered, assuming the different variables of state of that approximation as extra parameters at the parametrized microscale problem. In this work, the microscale internal variable distribution has been parametrized for the state variables at each node of the microscale discretization, thus a standard FE spatial approximation of the state variable is considered. A lower dimensional problem can be considered by approximating this spatial distribution, by regions and not for each node. This uncoupled procedure, gives the possibility to compute the state variable evolution by different ways at the macroscale problem. The main limitation of the uncoupled option is the large number of dimensions due to the parametrization with respect to the state variable associated to each node, and in consequence high numbers of terms for an accurate approximation of the parametrized displacement field over the RVE. However, this option is more flexible for the internal variable distribution at each increment of the macroscale problem due to the uncoupled nature of the procedure. This option can be implemented in problems where loading and unloading paths are different, and the microscale parametrized problem is totally independent of the state variable evolution/behavior.

To alleviate the parametrized microscale problem, a second option for problems with material non-linearity has been proposed, incorporating a parametrized microscale problem at each macroscale increment (FE-PGD). This option becomes advantageous when a large number of RVEs have to be analyzed for the macroscale problem, for example, substituting all the boundary value problems associated to each RVE by a single parametrized microscale problem, for further particularizations associated to a given RVE. This problem has a lower dimensionality compared to previous methods, because it is not parameterized with respect to the increment of time or state variables, but with respect to the RVEs at the macroscale discretization. The FE-PGD option can represent a suitable option for computer time saving when a very

Option	Macro Disp. x L_2 error	Macro Disp. y L_2 error	CPU Time Macroscale [**s**]	CPU Time "off-line"[**hrs**]
Uncoupled	3.6×10^{-3}	5.8×10^{-3}	360	17 (1000 terms)
FE-PGD	2.2×10^{-3}	3.3×10^{-3}	710	—

Table 3: Macroscale errors compared to a standard FE and computer time of the different schemes proposed for problems that present material nonlinearity.

fine discretization of the microscale model is required. As in the first option, this scheme is independent of the nature or expression that defines the variables of state behavior.

A comparison between the different schemes presented in this chapter is summarized in Table 3, where the same example for an isotropic damage model has been analyzed. Similar L_2 norm relative errors in displacement over the macroscale model for both directions have been observed for the three proposed schemes. These errors are due to the truncation of the approximation and the linear displacement approximation over the RVE boundary. Slightly lower relative errors have been computed for the FE-PGD option, this can be induced by the lower dimensionality of the microscale problem and therefore, a better PGD approximation for a relative low number of terms.

Computer time for the macroscale incremental problem for the uncoupled scheme was about 30% of the time it would take in a traditional FE. For the FE-PGD option, computer time for the same problem problem was 65% of the time for a full FE analysis, however, refining the microscale model from 39 to 92 elements, computer time reach 44% of the total time taken for a full FE analysis, besides an important reduction in computer memory requirement.

6. Acknowledgements

This work has been partially financed by Ascamm Technology Center in Barcelona. The authors gratefully acknowledge the financial support from the Spanish Ministry of Science and Technology, Diputación General de Aragón (DGA) and CIBER-BBN initiative.

Appendix A: Micro-Macro Transition

After performing the microscale step, the approximation of the displacement field over the RVE is obtained from the resulting basis function as:

$$\mathbf{u} = \sum_{i=1}^{I} \mathbf{a}_i(\mathbf{x}) \prod_{k=1}^{D} G_i^k(z_k) \tag{37}$$

The micro-macroscale information transmission is solved in the same manner as described in [16]. The internal force vector ($\mathbf{p}_{int}$) and the stiffness matrix ($\mathbf{K}$) are computed for each macroscale element with no more than particularizing the result of the parametrized microscale problem for values of the coordinates $\mathbf{x}^m$, the nodal displacements of the macroscopic RVE which represent the boundary conditions and of any other variable considered in the parametrization. Without loss of generality and to simplify the formulation, bilinear square elements have been considered here, although any other type of triangular or irregular quadrilateral may be also used after appropriate choice of the geometrical and displacement (boundary conditions) parameters. The expression for the internal force vector, we have:

$$\mathbf{p}_{int} = \int_{\Omega^{M_{el}}} \mathbf{B}^{M^T} \boldsymbol{\sigma}^{M_{el}} d\Omega^{M_{el}} = \sum_{n=1}^{N^m} \int_{\Omega_n^m} \mathbf{B}^{M^T} \mathbf{D}\boldsymbol{\varepsilon} \; d\Omega_n^m \tag{38}$$

where the strain operator matrix ($\mathbf{B}^M$) in this equation refers to the macroscale element and N^m represents the number of elements in the microscale domain. Substituting the strain approximation $\boldsymbol{\varepsilon}$ associated to the displacement field computed from the microscale step for a general microscale element n, we obtain:

$$\boldsymbol{\varepsilon} = \mathbf{B}^m(\mathbf{u}^M + \mathbf{u}^m) = \sum_{i=1}^{I} \mathbf{B}^m \mathbf{a}_n^i \prod_{k=1}^{D} G_{k_n}^i(z_k) \tag{39}$$

Here $\mathbf{B}^m$ is the strain operator matrix referring to the microscale element. Integrating now (38) onto each microscale element numerically (for example by using a Gauss-Legendre quadrature [38]) and assuming again square

shaped microscale elements we have:

$$\mathbf{p}_{int} = \sum_{n=1}^{N^m} \sum_{p=1}^{n_p} \sum_{q=1}^{n_q} \mathbf{B}^{M^T}(\xi_p^M, \eta_q^M)\mathbf{D}(x_p^M, y_q^M)\cdot \\ \cdot\Big[\sum_{i=1}^{I} \mathbf{B}^m(\xi_p^m, \eta_q^m)\mathbf{a}_n^i(\mathbf{x}) \prod_{k=1}^{D} G_{k_n}^i(z_k) W_p W_q\Big] |J_n^m| \tag{40}$$

where n_p and n_q are the number of integration points selected in each direction ξ and η, respectively. ξ_p^m and η_q^m are the Gaussian microscale coordinates defined in a normalized reference element for each Gaussian point (p, q); W_p and W_q represent the corresponding weights. As mentioned before, $\mathbf{B}^M$ is defined in the corresponding macroscale element, therefore, it must be evaluated in the global microscale coordinates (ξ_p^M and η_q^M) for each integration point. If the stiffness matrix $\mathbf{D}$ is spatially dependent, it must be evaluated in the global macroscale coordinate (x_p^M, y_q^M) corresponding to the integration point (p, q), so that (see Fig. 10):

$$\mathbf{D}(x_p^M, y_q^M) = \mathbf{D}(x_1^M + \xi_p^M, y_1^M + \eta_q^M) \tag{41}$$

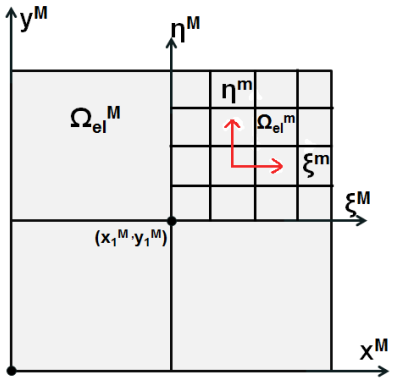

Figure 10: Macro and micro scale reference systems for the 2-D structural problem.

The explicit expression for the strain vector of a four node quadrilateral

microscale element n is:

$$\boldsymbol{\varepsilon} = \sum_{i=1}^{I} \begin{pmatrix} \frac{\partial N_1}{\partial x} & 0 & \frac{\partial N_2}{\partial x} & 0 & \frac{\partial N_3}{\partial x} & 0 & \frac{\partial N_4}{\partial x} & 0 \\ 0 & \frac{\partial N_1}{\partial y} & 0 & \frac{\partial N_2}{\partial y} & 0 & \frac{\partial N_3}{\partial y} & 0 & \frac{\partial N_4}{\partial y} \\ \frac{\partial N_1}{\partial y} & \frac{\partial N_1}{\partial x} & \frac{\partial N_2}{\partial y} & \frac{\partial N_2}{\partial x} & \frac{\partial N_3}{\partial y} & \frac{\partial N_3}{\partial x} & \frac{\partial N_4}{\partial y} & \frac{\partial N_4}{\partial x} \end{pmatrix} \begin{pmatrix} a_1^{x^i} \\ a_1^{y^i} \\ a_2^{x^i} \\ a_2^{y^i} \\ a_3^{x^i} \\ a_3^{y^i} \\ a_4^{x^i} \\ a_4^{y^i} \end{pmatrix} \prod_{k=1}^{D} G_k^i \tag{42}$$

where I represents the number of terms in the approximation. Here $a_{n_{el}}^{x^i}$ is the component of vector $\mathbf{a}^i$ corresponding to the degree of freedom defined in x direction of local microelement node n_{el}. The rest of functions G_k are obtained by evaluating the corresponding function obtained through the parametrized micro problem for the k-th parameter value, i.e. $G_{u_2^x}(u_0)$ is the value of the function associated to the displacement in x of vertex 2 evaluated for displacement u_0.

After computing the internal force vector for all macroscale elements by (40) and assembling them into the global internal force vector of the macroscale model, the stiffness matrix $\mathbf{K}$ is then computed in the same manner as in [16]. For bilinear quadrilateral elements we have:

$$\mathbf{K}^{el_M} = \begin{pmatrix} \frac{\partial \mathbf{p}_{int}}{\partial u_1^x} & \frac{\partial \mathbf{p}_{int}}{\partial u_1^y} & \frac{\partial \mathbf{p}_{int}}{\partial u_2^x} & \frac{\partial \mathbf{p}_{int}}{\partial u_2^y} & \frac{\partial \mathbf{p}_{int}}{\partial u_3^x} & \frac{\partial \mathbf{p}_{int}}{\partial u_3^y} & \frac{\partial \mathbf{p}_{int}}{\partial u_4^x} & \frac{\partial \mathbf{p}_{int}}{\partial u_4^y} \end{pmatrix} \tag{43}$$

The derivative of the internal force vector with respect to displacements different from u_1^x and u_1^y can be obtained as follows: let us consider, for example, the derivative with respect to u_2^x, substituting the internal force expression (38) with the strain expression (39) in $\partial \mathbf{p}_{int}/\partial u_2^x$ and considering the variables chosen for the displacement approximation, the stiffness matrix column associated to the derivative with respect to u_2^x for a macroscale element can be expressed as:

$$\begin{aligned} \frac{\partial \mathbf{p}_{int}}{\partial u_2^x} = \sum_{n=1}^{N^m} \int_{\Omega_n^m} \mathbf{B}^{T^M} \mathbf{D} \sum_{i=1}^{I} \mathbf{B}^m \mathbf{a}_n^i(\mathbf{x}) \frac{\partial C1_i(u_2^x)}{\partial u_2^x} \cdot \\ \cdot C2_i(u_3^x) C3_i(u_4^x) B1_i(u_2^y) B2_i(u_3^y) B3_i(u_4^y) \end{aligned} \tag{44}$$

The functions depending on the vertex displacements of the microscale domain (RVE) are expressed in discrete form; therefore, the derivative of function $\partial C1_l(u_2^x)/\partial u_2^x$ at a value $u_2^{x^0}$ can be expressed as:

$$\frac{\partial C1_i(u_2^{x^0})}{\partial u_2^x} = \frac{C1_i(u_2^{x^{z+1}}) - C1_i(u_2^{x^z})}{\ell^{ln}} \tag{45}$$

where, as shown in Fig. 11, $u_2^{x^{z+1}}$ and $u_2^{x^z}$ are the nodal values of $C1_i$ associated to the one-dimensional element in the u_2^x discretization to which $u_2^{x^0}$ belongs to.

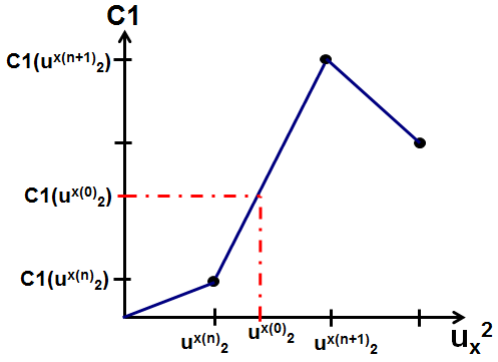

Figure 11: One-dimensional piecewise linear representation of function $C1(u_2^x)$.

References

[1] C. McVeigh, W. K. Liu, Linking microstructure and properties through a predictive multiresolution continuum, Computer Methods In Applied Mechanics and Engineering 197 (41-42) (2008) 3268–3290.

[2] R. de Borst, Challenges in computational materials science: Multiple scales, multi-physics and evolving discontinuities, Computational Materials Science 43 (1) (2008) 1–15.

[3] T. Zohdi, P. Wriggers, An introduction to computational micromechanics, Springer, 2005.

[4] T. J. R. Hughes, Multiscale phenomena - greens-functions, the dirichlet-to-neumann formulation, subgrid scale models, bubbles and the origins of stabilized methods, Computer Methods In Applied Mechanics and Engineering 127 (1-4) (1995) 387–401.

[5] A. M. Amini, D. Dureisseix, P. Cartraud, Multi-scale domain decomposition method for large-scale structural analysis with a zooming technique: Application to plate assembly, International Journal For Numerical Methods In Engineering 79 (4) (2009) 417–443.

[6] J. Pinho-da Cruz, J. A. Oliveira, F. Teixeira-Dias, Asymptotic homogenisation in linear elasticity. part i: Mathematical formulation and finite element modelling, Computational Materials Science 45 (4) (2009) 1073–1080.

[7] P. Kanoute, D. Boso, J. Chaboche, B. Schrefler, Multiscale methods for composites: A review, Archives of Computational Methods in Engineering 16 (1) (2009) 31–75.

[8] F. Feyel, Multiscale FE^2 elastoviscoplastic analysis of composite structures, Computational Materials Science 16 (1-4) (1999) 344–354.

[9] P. W. Chung, K. K. Tamma, R. R. Namburu, Asymptotic expansion homogenization for heterogeneous media: computational issues and applications, Composites Part A-applied Science and Manufacturing 32 (9) (2001) 1291–1301.

[10] J. A. Oliveira, J. Pinho-da Cruz, F. Teixeira-Dias, Asymptotic homogenisation in linear elasticity. part ii: Finite element procedures and multiscale applications, Computational Materials Science 45 (4) (2009) 1081–1096.

[11] P. M. Suquet, Homogenization methods in the mechanics of solids, Journal of Rheology 29 (2) (1985) 235–235.

[12] J. Fish, K. Shek, M. Pandheeradi, M. S. Shephard, Computational plasticity for composite structures based on mathematical homogenization: Theory and practice, Computer Methods In Applied Mechanics and Engineering 148 (1-2) (1997) 53–73.

[13] F. Feyel, J. L. Chaboche, FE^2 multiscale approach for modelling the elastoviscoplastic behaviour of long fibre sic/ti composite materials, Computer Methods In Applied Mechanics and Engineering 183 (3-4) (2000) 309–330.

[14] F. Feyel, A multilevel finite element method (FE^2) to describe the response of highly non-linear structures using generalized continua, Computer Methods In Applied Mechanics and Engineering 192 (28-30) (2003) 3233–3244.

[15] A. Abdulle, Analysis of a heterogeneous multiscale fem for problems in elasticity, Mathematical Models & Methods In Applied Sciences 16 (4) (2006) 615–635.

[16] F. El Halabi, D. González, A. Chico-Roca, M. Doblaré, FE^2 multiscale in linear elasticity based on parametrized microscale models using proper generalized decomposition, Computer Methods in Applied Mechanics and Engineering 257 (0) (2013) 183–202.

[17] A. Nouy, A. Clement, F. Schoefs, N. Moes, An extended stochastic finite element method for solving stochastic partial differential equations on random domains, Computer Methods In Applied Mechanics and Engineering 197 (51-52) (2008) 4663–4682.

[18] A. Nouy, Recent developments in spectral stochastic methods for the numerical solution of stochastic partial differential equations, Archives of Computational Methods In Engineering 16 (3) (2009) 251–285.

[19] A. Nouy, O. P. Le Maitre, Generalized spectral decomposition for stochastic nonlinear problems, Journal of Computational Physics 228 (1) (2009) 202–235.

[20] A. Leygue, E. Verron, A first step towards the use of proper general decomposition method for structural optimization, Archives of Computational Methods In Engineering 17 (4) (2010) 465–472.

[21] A. Ammar, B. Mokdad, F. Chinesta, R. Keunings, A new family of solvers for some, classes of multidimensional partial differential equations encountered in kinetic theory modeling of complex fluids, Journal of Non-newtonian Fluid Mechanics 139 (3) (2006) 153–176.

[22] A. Ammar, B. Mokdad, F. Chinesta, R. Keunings, A new family of solvers for some classes of multidimensional partial differential equations encountered in kinetic theory modelling of complex fluids: Part ii: Transient simulation using space-time separated representations, Journal of Non-Newtonian Fluid Mechanics 144 (2-3) (2007) 98–121.

[23] D. González, A. Ammar, F. Chinesta, E. Cueto, Recent advances on the use of separated representations, International Journal For Numerical Methods In Engineering 81 (5) (2010) 637–659.

[24] A. Nouy, A priori model reduction through proper generalized decomposition for solving time-dependent partial differential equations, Computer Methods In Applied Mechanics and Engineering 199 (23-24) (2010) 1603–1626.

[25] P. Ladeveze, D. Neron, P. Gosselet, On a mixed and multiscale domain decomposition method, Computer Methods in Applied Mechanics and Engineering 196 (8) (2007) 1526–1540.

[26] D. Neron, P. Ladeveze, Proper generalized decomposition for multiscale and multiphysics problems, Archives of Computational Methods In Engineering 17 (4) (2010) 351–372.

[27] F. Chinesta, A. Ammar, E. Cueto, Recent advances and new challenges in the use of the proper generalized decomposition for solving multidimensional models, Archives of Computational Methods In Engineering 17 (4) (2010) 327–350.

[28] A. Ammar, F. Chinesta, E. Cueto, M. Doblaré, Proper generalized decomposition of time-multiscale models, International Journal for Numerical Methods in Engineering. (2012) 569–596

[29] O. C. Zienkiewicz, R. L. Taylor, J. Zhu, The Finite Element Method: Its Basis and Fundamentals, 5th Edition, Vol. 1, Butterworth-Heinemann, 2000.

[30] K. Garikipati, T. J. R. Hughes, A study of strain localization in a multiple scale framework - the one-dimensional problem, Computer Methods In Applied Mechanics and Engineering 159 (3-4) (1998) 193–222.

[31] J. I. McCool, The three-parameter weibull distribution, in: Using the Weibull Distribution, John Wiley & Sons, Inc., 2012, pp. 298–312.

[32] K. Matous, M. G. Kulkarni, P. H. Geubelle, Multiscale cohesive failure modeling of heterogeneous adhesives, Journal of the Mechanics and Physics of Solids 56 (4) (2008) 1511–1533.

[33] K. Matous, Damage evolution in particulate composite materials, International Journal of Solids and Structures 40 (6) (2003) 1489–1503.

[34] D. González, E. Cueto, F. Chinesta, Real-time direct integration of reduced solid dynamics equations, International Journal for Numerical Methods in Engineering 99 (9) (2014) 633–653.

[35] S. Volkwein, Model reduction using proper orthogonal decomposition. Lecture Notes, Institute of Mathematics and Scientific Computing, University of Graz. (2011) see http://www.uni-graz.at/imawww/volkwein/POD.pdf.

[36] J. Simo, J. Ju, Strain and stress-based continuum damage models. i. formulation, International Journal of Solids and Structures 23 (7) (1987) 821–840.

[37] J. Ju, On energy-based coupled elastoplastic damage theories: Constitutive modeling and computational aspects, International Journal of Solids and Structures 25 (7) (1989) 803–833.

[38] J. Stoer, R. Bulirsch, Introduction to Numerical Analysis, 3rd Edition, Vol. 12 of Texts in Applied Mathematics„ Springer, 2002.

[39] N. Faber, R. Bro, P. K. Hopke, Recent developments in candecomp/parafac algorithms: a critical review, Chemometrics and Intelligent Laboratory Systems 65 (1) (2003) 119–137.

[40] J. Carroll, J.-J. Chang, Analysis of individual differences in multidimensional scaling via an n-way generalization of eckart-young decomposition 35 (3) (1970) 283–319.